Open access • Journal Article • DOI:10.1063/1.4904837

One channel defect imaging in a reverberating medium — Source link

S. Rodriguez, S. Rodriguez, Martin Veidt, Michel Castaings ...+2 more authors

Institutions: ParisTech, Cooperative Research Centre, University of Queensland

Published on: 19 Dec 2014 - Applied Physics Letters (AIP Publishing)

Topics: Transducer, Physical acoustics, Surface acoustic wave sensor, Acoustic wave equation and Surface acoustic wave

One channel defect imaging in a reverberating medium

S. Rodriguez, M. Veidt, M. Castaings, Eric Ducasse, and M. Deschamps

Citation: Applied Physics Letters **105**, 244107 (2014); doi: 10.1063/1.4904837
View online: http://dx.doi.org/10.1063/1.4904837
View Table of Contents: http://scitation.aip.org/content/aip/journal/apl/105/24?ver=pdfcov
Published by the AIP Publishing

One channel defect imaging in a reverberating medium

S. Rodriguez,[1,2,a)] M. Veidt,[3] M. Castaings,[1] Eric Ducasse,[1] and M. Deschamps[1]
[1]*Univ. Bordeaux, I2M, UMR 5295, F-33400 Talence, France; CNRS, I2M, UMR 5295, F-33400 Talence, France; Bordeaux INP, I2M, UMR 5295, F-33400 Talence, France; and Arts et Métiers Paris Tech, I2M, UMR 5295, F-33400 Talence, France*
[2]*Cooperative Research Centre for Advanced Composite Structures, 1/320 Lorimer Street, Port Melbourne, Victoria 3207, Australia*
[3]*School of Mechanical and Mining Engineering, The University of Queensland, Brisbane St Lucia, Queensland 4072, Australia*

(Received 17 October 2014; accepted 3 December 2014; published online 19 December 2014)

This letter presents an acoustic one-channel location system that takes advantage of the multiple reflections occurring in the reverberating medium under investigation. Experimental results are obtained with guided waves propagating in a bounded aluminum plate. The plate is so designed that there is no direct propagation path between the single transducer and the region of interest in the plate. In that manner, the two-dimensional image obtained in the region of interest is only based on the reverberated acoustic field measured with the single fixed transducer. The method is based on the application of topological optimization methods to wave-based location problems and on a preliminary calibration of the whole system. This calibration mainly consists in measuring the impulse response of the transducer in the region of interest before any object or defect is present. The calibration is here performed with a Laser Doppler velocimeter. The experimental results obtained with this one-channel topological imaging method show accurate location of a single small defect and of multiple small defects, with a resolving power below the wavelength. © *2014 AIP Publishing LLC*.
[http://dx.doi.org/10.1063/1.4904837]

Location of impact noise sources and defects in reverberating media can be performed with several transducers using triangulation-like or transducer array methods. These methods however only rely on the wave propagating directly from the source to the transducer, the so-called ballistic wave. All the remaining physical information contained in the multiple reflected wave field is discarded. Time reversal process permits to take advantage of this information for locating the noise source generated by an impact.[1] It results in a one-channel accurate location method.[2] Localizing an impact noise source and localizing a defect are two different problems. The impact experiment only requires the wave field to be measured, since the impact is the noise source, whereas the defect location requires the wave field to be emitted and measured by the user. Furthermore, the impact experiment does not modify the investigated medium, whereas the appearance of a defect does. This mechanical modification may imply changes in the way waves propagate in the medium during the experiment. The influence of the presence of a localized defect in a reverberating medium has been extensively investigated, for example by Leyla *et al.*,[3] but no one-channel experimental defect location method has been proposed yet. This is the purpose of the present work.

The interest of multiple reflections can be explained as follows. Let us consider a sensor in a domain bounded by a half space reflective boundary condition that behaves like a mirror. The boundary condition provides a supplementary virtual sensor that would be located on the other side of the mirror. If the imaging process can properly deal with the boundary condition, the presence of the virtual sensor enhances the imaging process in the way that the image is obtained as if there were two sensors instead of one. Considering now a fully bounded domain without any attenuation, the multiple reflections theoretically provide an infinite number of virtual sensors and the resolution of the imaging process converges to the diffraction limit given by half the wavelength. The present experiments are led in a strongly reverberating medium; namely, in a bounded domain with small attenuation. Using the physical information measured with a single sensor in such a domain is thus equivalent to the investigation of an unbounded domain with a very large number of sensors surrounding the scatterers. The challenge lies in the proper processing of the whole signal that is the result of hundreds of reflections.

Since 2004, topological optimization methods have been applied to solve inverse scattering problems in elastodynamics,[4] acoustics,[5] and electromagnetism.[6] Initially developed for shape optimization, these methods rely on the sensitivity study of a misfit function with respect to the introduction of a localized defect in the so-called reference medium. This topological sensitivity (or topological gradient) can be explicitly expressed as a function of two wave fields obtained in the reference medium. Both wave fields are usually obtained with numerical simulations and are referred as to the solutions of the direct and the adjoint problems, respectively. Using a reference medium as close as possible to the experimental medium and an appropriate numerical tool, the method is experimentally applied with traditional emitter/receiver transducers and leads to accurate location and imaging of various defects.[7–9] So far, the method has been applied with infinite or semi-infinite reference media, as well as by

[a)]Author to whom correspondence should be addressed. Electronic mail: samuel.rodriguez@u-bordeaux.fr.

taking into account the first reflections at the edge of a bounded domain.[10] As the topological gradient is the misfit function derivative with respect to the defect location, it typically takes very negative values at locations of the reference medium where inserting a defect tends to strongly decrease the misfit function. Thus, local minima correspond to defect locations and an imaging function is directly given by the topological sensitivity. It highlights all the differences between the experimental and the reference media.

For representation purposes, a slightly modified formulation of the gradient may be preferred.[8] In this paper, the formulation used leads to maxima of the imaging function at the locations of the defects. It is given by

$$T(x,y) = \left| \int_{\mathbb{R}^+} U(x,y,\omega)\, V(x,y,\omega) d\omega \right|, \tag{1}$$

where the capital letters U and V correspond to the time Fourier transforms of the two normal displacement fields u and v at the surface of the plate, respectively, and ω stands for the angular frequency. Fields u and v are the solutions of the so-called direct and adjoint problems,[9] respectively. It has to be noted that (1) is in general given for three-dimensional displacement vector depending on three-dimensional coordinates. The study is here restricted to the normal displacement of the surface of the plate. Plotting the function $T(x,y)$ gives an image in the plane $(\boldsymbol{x},\boldsymbol{y})$.[7–9]

Let us assume that a punctual source is located at the point $(x_0,\, y_0)$. Knowing, in the absence of defect, the acoustic impulse response $h(x,y,t)$ associated to this source, the two fields u and v can be expressed, respectively, by

$$u(x,y,t) = h(x,y,t) * u_s(t), \tag{2a}$$

$$v(x,y,t) = h(x,y,t) * r(-t), \tag{2b}$$

where $u_s(t)$ is the normal displacement produced by the transducer and $r(t)$ the residual. In the present case, i.e., for a single emitter/receiver transducer, the residual is given by

$$r(t) = u(x_0,\, y_0, t) - u_{exp}(t)\,, \tag{3}$$

where $u_{exp}(t)$ expresses the normal field measured at the location $(x_0,\, y_0)$ in the experiments (eventually in the presence of defects) and $u(x_0,y_0,t)$ corresponds to the field defined in (2a) (in the absence of defect) at the same location. The residual reveals the presence of possible defects. If it equals zero at all time samples, there is no defect in the plate and consequently the imaging function equals zero at all locations. It has to be noted that the source of the adjoint problem is the time-reversed residue. Despite this similarity, topological imaging differs from the time-reversed based pulse-echo methods on two aspects. First, the time-reversed based methods rely on the time-reversed measurement, not the residue. Second, they require to look for the spatio-temporal maxima of the back-propagated wavefield. This last step is unnecessary in topological imaging since the product of direct and adjoint fields directly provide the locations of the defects. In concrete terms, using the present formulation of topological imaging for the fixed transducer position, imaging a plate structure consists in the computation of the two fields u and v trough the impulse response $h(x,y,t)$.

The plate under study is presented in Fig. 1. The specimen is a 600 × 600 mm and 1.6 mm thick aluminum plate that has been sawn along half of its length. In the present experiment, the sawn line separates the investigated area and the transducer, so that no ballistic wave propagates between them. Thus, the results will exclusively rely on multiple-reflected waves. The method can deal with ballistic waves like in the previous experimental applications[7–9] but suppressing them allows to demonstrate that they are not necessary for the reverberating medium inspection. The transducer is a 5 mm in diameter piezoelectric sensor adhesively bonded to one side of the plate at the position $(x_0,\, y_0)$. It is connected to a one-channel Panametrics 5077 pulser/receiver device. The output impedance is tuned to match the sensor whose frequency range extends from 100 to 300 kHz. Considering this frequency-thickness range and the transducer size, the source is assumed punctual. It generates guided waves that propagate along the plate in all directions of the $(\boldsymbol{x},\boldsymbol{y})$ plane. In the frequency-thickness range of interest, only the A_0 guided mode (flexural mode) has a significant out of plane displacement. The displacement field measured with a Laser Doppler Velocimeter (LDV) in the absence of defect thus corresponds to the propagation of the A_0 mode in the reference medium.

To perform the image computations following (1) and (2), in addition to the perfect knowledge of the reference medium, numerical methods such as finite elements are required due to the complexity of the investigated structure. However, in this work, the experimental measurement of the impulse response is taken as an alternative to numerical computations. This implies that the reference medium is thus the defect-free experimental medium, and not a numerical medium. It also implies the measurement of the plate displacement generated by the source over a 2D area. It is not necessary to scan the whole sample surface. This inspection can be reduced to a smallest region, called the Region of Interest (ROI). Of course, in this case, the image will also be restricted to the ROI. The transducer does not necessarily belong to the ROI, where defects are assumed to be located. The ROI has dimensions 90 mm × 90 mm and the origin of the axes is set to $(0,0)$ at the bottom left of the ROI. The

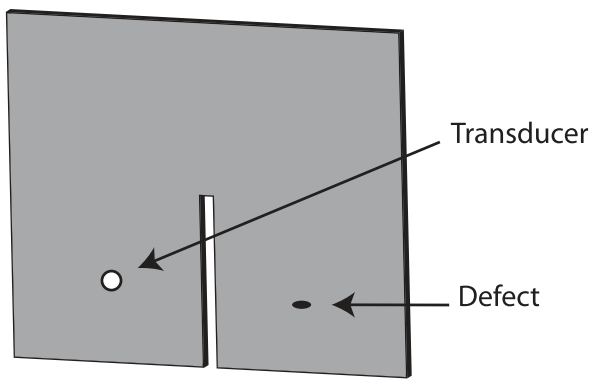

FIG. 1. The specimen under study. A single transducer is used to emit guided waves and to measure the response of the medium where a defect may appear.

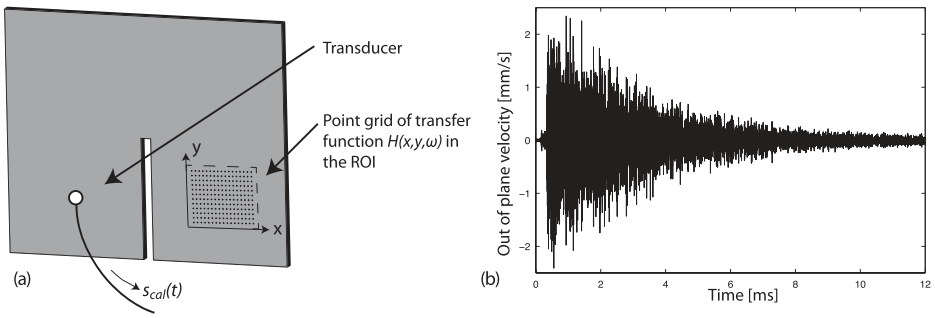

FIG. 2. Calibration of the plate. (a) Measurement of the displacement field $u(x, y, t)$ in the ROI with LDV and of the response $s_{cal}(t)$ obtained with the transducer. (b) A typical out of plane velocity signal measured with the LDV. It is then integrated to get the displacement field.

transducer is excited by a broadband signal that remains the same at all stages of the method.

The first step of the method is thus the measurement of $h(x, y, t)$. Referring to (2a), it can be obtained in the absence of defect by the time-domain deconvolution of the displacement field $u(x, y, t)$ measured in the ROI by the displacement generated by the transducer at the transducer location $u_s(t)$. Writing this relation in the frequency domain leads to the transfer function

$$H(x, y, \omega) = U(x, y, \omega)/U_s(\omega), \tag{4}$$

where H, U, and U_s are the time-domain Fourier Transforms of h, u, and u_s, respectively. The out of plane displacement field $u(x, y, t)$ is measured in the ROI of the defect-free medium using the LDV (Fig. 2).

In order to capture all the multiple reflected waves, the acquisition time is set to 12 ms. The ROI is scanned along both directions with a 3 mm space step (Fig. 2(a)). As an example, the out of plane displacement measured at coordinates (0,0) is presented in Fig. 2(b).

The reverberation in the medium is clearly emphasized by the slow decrease of the magnitude of the multiple-reflected waves. It has to be noted that taking the half length of the plate $L = 300$ mm as the characteristic length of the medium, the time of analysis 12 ms corresponds to a propagation on a distance of about 100 L. $u_s(t)$ is the displacement generated by the transducer at the transducer location during the emission. It thus excludes the multiple reflected waves and it is measured with the LDV at the transducer location on the other side of the plate. As the displacement field generated by the transducer has a limited bandwidth and is not comparable with a Dirac function, the deconvolution step described in (4) is mandatory.

Then, calculating the residual (3) requires the acoustic field at the transducer location in the reference medium $u(x_0, y_0, t)$. As the displacement measured with a piezo transducer in the experiments will be subtracted from $u(x_0, y_0, t)$, $u(x_0, y_0, t)$ is also measured with the very same fixed transducer (Fig. 2). The signal obtained is noted $s_{cal}(t)$ where the subscript *cal* corresponds to calibration. Considering the small size of the transducer in comparison with the wavelength, the measurement is assumed punctual and $s_{cal}(t) \approx \alpha\, u(x_0, y_0, t)$, where α is a proportionality coefficient. The measurements of the impulse response $h(x, y, t)$ and of the signal $s_{cal}(t)$ can be considered as a global acoustic and electronic calibration of the system that includes all the wave phenomena that may exist in the inspected structures: multiple reflection/refraction, inhomogeneities, anisotropy, wave attenuation, etc. It has to be emphasized that this calibration is performed once and for all in the reference medium, i.e., in the absence of defect.

Let us now present the localization experiments and the underlying hypothesis. The mathematical optimization problem that is the basis of the method considers the diffraction of the incident field by a single small defect. Thus, in experimental applications where the Born approximation is valid, the superposition principle guarantees that big objects or a high number of small objects can be imaged simultaneously. In strongly reverberating media, the Born approximation is guaranteed only for a single defect. It may be invalid for a small number of scatterers because the hundreds of reflections provided by the edges may lead to non-negligible acoustic interactions between the scatterers themselves. In the present experiments, the modification of the medium consists in coupling one or several 3 mm in diameter, 2 mm in thickness, and 0.1 g metal cylinder(s) to one face of the plate in the ROI (Fig. 1). These scatterers are small compared to the wavelength and the localization results are satisfactory up to three scatterers. With a higher number of objects or with objects that are not small compared to the wavelength, the results obtained were not conclusive. The authors think that the Born approximation was in these cases invalid.

The only experimental data required to build the image of the defects in the ROI is the response of the modified

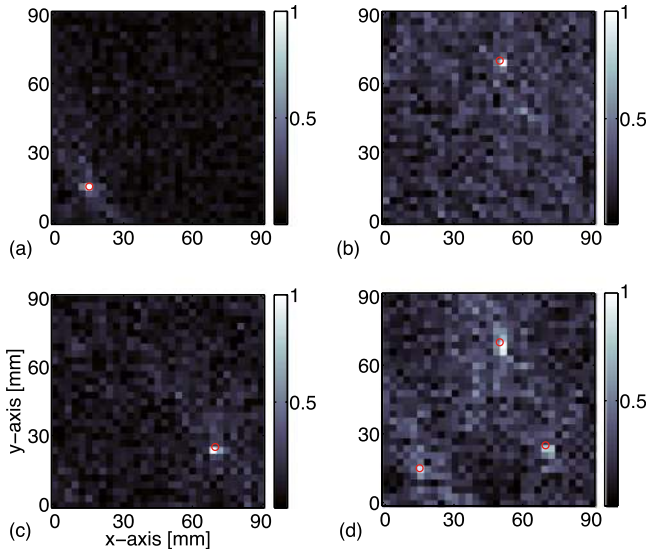

FIG. 3. Images of defects at different locations and corresponding real locations. Dimensions are given in mm. (a) The defect is located at (15,15). (b) The defect is located at (50,70). (c) The defect is located at (70,25). (d) Three defects are located at (15,15), (50,70), and (70,25), respectively.

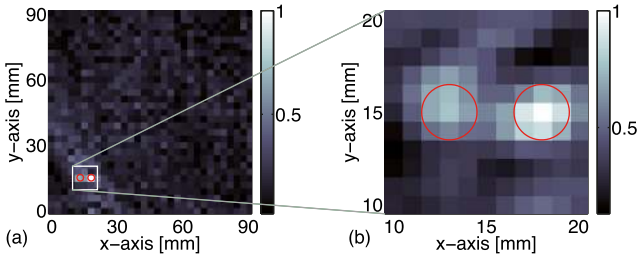

FIG. 4. Image of the two close defects, respectively, located at coordinates (13,15) and (18,15). (a) Image obtained with the calibration transfer functions measured every 3 mm. (b) Image obtained with the calibration transfer functions measured every 1 mm in a small part of the ROI.

medium to the excitation provided by the piezo transducer. This measurement is performed with the piezo (necessarily at the location (x_0, y_0)) and corresponds to the normal field $u_{exp}(t)$ introduced in the residual expression (3). It is noted $s_{exp}(t)$ and the same proportionality relation between the displacement and the signal measured as for the calibration is obtained: $s_{exp}(t) \approx \alpha\, u_{exp}(t)$. Thus, a good approximation for the residual is given by

$$r(t) \approx \frac{1}{\alpha}\left(s_{cal}(t) - s_{exp}(t)\right). \tag{5}$$

Noting that the images are normalized, the proportionality coefficient α is neglected. Then, all the data required to compute the image with (1), (2), and (5) are now obtained.

Different locations were tested for single defect studies (Figs. 3(a)–3(c)) and for a three-defect measurement (Fig. 3(d)). The local maxima of the imaging functions correspond to the location of the defects estimated with the method. The real locations of the defects are superimposed to the images and indicated by 3 mm in diameter red circles. The different defects are clearly identified and accurately located, even in the presence of several defects. Still, the contrast of the image with the three defects (Fig. 3(d)) is lower than for single defect experiments. The authors consider that this configuration is at the limit of validity of the Born approximation in the present experimental conditions, and thus the imaging artefacts tend to be of similar magnitude with the localization spots.

The size of the spot indicating the defect is remarkably small compared to the 8 mm wavelength at the central frequency. In order to investigate the resolving power of the method, a finer 1 mm grid was also measured with the LDV during the calibration process, between the coordinates (10,10) and (20,20) of the ROI. The image of two defects located at (13,15) and (18,15) is presented in Fig. 4. The two defects are clearly distinguished in the image (Fig. 4(b)). The 5 mm separating the two defects corresponds to 0.62 and 0.8 times the wavelength at the central and the maximum frequencies, respectively.

The experimental results demonstrate that topological imaging allows the location of small objects present in a reverberating medium with a single fixed transducer. Using the transducer as both emitter and receiver, one to three objects were located with an excellent resolution. It also demonstrates that the topological imaging formalism is adapted to complex media and that this complexity can be taken into account with the experimental evaluation of the impulse response spatially restricted to the region of interest. These results may lead to significant changes in the way Structural Health Monitoring is managed. For example, one or several transducers may be embedded in the structures with random locations and be used for monitoring the appearance of defects in the structure, even in hidden places. Furthermore, this method is adapted to complex geometries and structures as linear propagation and validity of Born approximation are the only required hypotheses.

This work was undertaken as part of a CRC-ACS research program, established and supported under the Australian Government's Cooperative Research Centers Program.

[1]C. Draeger and M. Fink, Phys. Rev. Lett. **79**, 407 (1997).
[2]R. K. Ing, N. Quieffin, S. Catheline, and M. Fink, Appl. Phys. Lett. **87**, 204104 (2005).
[3]N. A. Leyla, E. Moulin, and J. Assaad, J. Appl. Phys. **110**, 084906 (2011).
[4]B. B. Guzina and M. Bonnet, Q. J. Mech. Appl. Math. **57**, 161 (2004).
[5]A. Malcolm and B. Guzina, Wave Motion **45**, 821 (2008).
[6]M. Masmoudi, J. Pommier, and B. Samet, Inverse Prob. **21**, 547 (2005).
[7]N. Dominguez and V. Gibiat, Ultrasonics **50**, 367 (2010).
[8]S. Rodriguez, P. Sahuguet, V. Gibiat, and X. Jacob, Ultrasonics **52**, 1010 (2012).
[9]S. Rodriguez, M. Deschamps, M. Castaings, and E. Ducasse, Ultrasonics **54**, 1880 (2014).
[10]R. Tokmashev, A. Tixier, and B. B. Guzina, Inverse Prob. **29**, 125005 (2013).